BJR

Received: 18 February 2015 | Revised: 7 April 2015 | Accepted: 15 April 2015

doi: 10.1259/bjr.20150147

Cite this article as:
Meissnitzer T, Seymer A, Keinrath P, Holzmannhofer J, Pirich C, Hergan K, et al. Added value of semi-quantitative breast-specific gamma imaging in the work-up of suspicious breast lesions compared to mammography, ultrasound and 3-T MRI. Br J Radiol 2015;88:20150147.

FULL PAPER

Added value of semi-quantitative breast-specific gamma imaging in the work-up of suspicious breast lesions compared to mammography, ultrasound and 3-T MRI

[1]T MEISSNITZER, MD, [2]A SEYMER, DSc, [3]P KEINRATH, MD, [3]J HOLZMANNHOFER, BSc, [3]C PIRICH, MD, [1]K HERGAN, MD and [1]M W MEISSNITZER, MD

[1]Department of Radiology, Paracelsus Medical University Salzburg, Salzburg, Austria
[2]Department of Sociology and Cultural Science, University of Salzburg, Salzburg, Austria
[3]Department of Nuclear Medicine, Paracelsus Medical University Salzburg, Salzburg, Austria

Address correspondence to: Dr Thomas Meissnitzer
E-mail: *thomas.meissnitzer@gmail.com*

Objective: To prospectively analyse the diagnostic value of semi-quantitative breast-specific gamma imaging (BSGI) in the work-up of suspicious breast lesions compared with that of mammography (MG), breast ultrasound and MRI of the breast.
Methods: Within a 15-month period, 67 patients with 92 breast lesions rated as Category IV or V according to the breast imaging reporting and data system detected with MG and/or ultrasound were included into the study. After the injection of 740–1110 MBq of Technetium-99m (^{99m}Tc) SestaMIBI intravenously, scintigrams were obtained in two projections comparable to MG. The BSGI was analysed visually and semi-quantitatively by calculating a relative uptake factor (*X*). With the exception of two patients with cardiac pacemakers, all patients underwent 3-T breast MRI. Biopsy results were obtained as the reference standard in all patients. Sensitivity, specificity, positive- and negative-predictive values, accuracy and area under the curve were calculated for each modality.
Results: Among the 92 lesions, 67 (72.8%) were malignant. 60 of the 67 cancers of any size were detected by BSGI with an overall sensitivity of 90%, only exceeded by ultrasound with a sensitivity of 99%. The sensitivity of BSGI for lesions <1cm declined significantly to 60%. Overall specificity of ultrasound was only 20%. Specificity, accuracy and positive-predictive value were the highest for BSGI (56%, 80% and 85%, respectively). *X* was significantly higher for malignant lesions (mean, 4.27) and differed significantly between ductal types (mean, 4.53) and the other histopathological entities (mean, 3.12).
Conclusion: Semi-quantitative BSGI with calculation of the relative uptake factor (*X*) can help to characterize breast lesions. BSGI negativity may obviate the need for biopsy of breast lesions >1cm with low or intermediate prevalence for malignancy.
Advances in knowledge: Compared with morphological imaging modalities, specificity, positive-predictive value for malignancy and accuracy were the highest for BSGI in our study. BSGI negativity may support the decision not to biopsy in selected lesions with a low or low-to-moderate pre-test probability for malignancy.

Tissue characterization is fundamental in the assessment of suspicious breast lesions. Based on specific imaging findings, breast lesions are selected for biopsy, as histopathological examination is the essential part of a comprehensive diagnosis and the basis for an individually adjusted therapy.

An imaging modality used in this setting should be rapidly available and highly accurate, minimizing the need for additional examinations and preventing unnecessary biopsies of benign lesions. Being aware of the limitations of the established imaging modalities, such as mammography (MG), ultrasound and MRI of the breast, we implemented breast-specific gamma imaging (BSGI) as an adjunct imaging modality in the work-up of suspicious breast lesions.[1] BSGI as functional imaging modality visualizes metabolic alterations in contrast to MG, ultrasound and MRI, which show primarily structural breast changes as morphological imaging modalities.

The BSGI has been suggested to overcome some limitations of scintimammography as described in the latest version of the European Association of Nuclear Medicine (EANM) breast scintigraphy guidelines.[2] In scintimammography, it was impossible to create images comparable to MG because

standard gamma cameras were used.[3] In contrast to BSGI, prone positioning required for scintimammography prevented direct contact of the breast and the detector and compromised the spatial resolution.[4] Edge effects at the border of the large single crystal of sodium iodine (NaI) resulted in a significant "dead space".[5]

In contrast to former studies, such as Tadwalkar et al,[6] we implemented BSGI in the assessment of suspicious breast lesions detected initially with MG and breast ultrasound. As a result, we were able to prospectively analyse the performance of BSGI in the assessment of suspicious breast lesions and to compare the results to the other well-established imaging modalities in a large series of patients in a breast cancer centre. The benefit of an easily calculated uptake factor (*X*) in addition to visual evaluation was also assessed.

METHODS AND MATERIALS

This prospective study was approved by the local ethics committee. Written informed consent was obtained from each patient. The criteria for inclusion into the study were newly diagnosed breast lesions of the Categories IV and V according to the breast imaging reporting and data system (BI-RADS®), patient age above 50 years and informed consent. A total of 67 females with 92 lesions were included in the study within a 15-month period from January 2013 to March 2014. 37 patients were asymptomatic, so lesions were detected in screening examinations. 30 patients were symptomatic complaining about breast pain or a lump in the breast. Lesions were detected initially either in external examinations and referred to our assessment centre or at our institution, using MG and ultrasound. Those lesions, which were detected in external examinations, were re-evaluated by a specialist in radiology and nuclear medicine (TM) with 8 years' experience in breast imaging. All patients, in whom the re-evaluation at our institution confirmed the presence of a BI-RADS IV or V lesion, were consecutively included in the study. In addition, all patients with BI-RADS IV and V lesions detected at our institution with MG and ultrasound were also consecutively included into the study by one examiner (TM).

The assessment of the breast lesions was performed equally in all patients. After clinical examination, evaluation of mammograms and ultrasound examination, BSGI was performed at the presentation. In all patients, MRI was performed within 10 days and prior to biopsy. Two patients could not be examined with MRI owing to cardiac pacemakers. Each lesion was characterized separately in every imaging modality according to the BI-RAD system by the same examiner (TM), who was not blinded to the other imaging modalities.[7]

The reading order of the imaging modalities was performed as follows: firstly MG, secondly ultrasound and thirdly BSGI, which was performed in all patients at the day of presentation at our institution. Finally, MRI was the last modality to be performed and interpreted. This reading order ensured that BSGI interpretation could not be biased by breast MRI.

BSGI interpretation was performed by TM and another specialist in nuclear medicine (PK), also with 8 years' experience in breast imaging. For BSGI consensus, reading was performed by the two examiners with regard to the presence or absence of increased tracer uptake and the measurement of a relative uptake factor. For BSGI interpretation, imaging findings of MG and ultrasound were available to both examiners (TM and PK). Final BI-RADS rating corresponded to the maximum BI-RADS category, regardless of the modality and including MRI findings. Finally, all lesions were biopsied, and biopsy results were the reference standard. Evaluation of all included lesions under identical conditions could be ensured by this standardized approach.

Figure 1. Positioning of regions of interest (ROIs) in the scintigrams to calculate relative uptake (*X*). A, area; avg, average; d, diameter; max, maximum; min, minimum; sd, standard deviation; U, circumference.

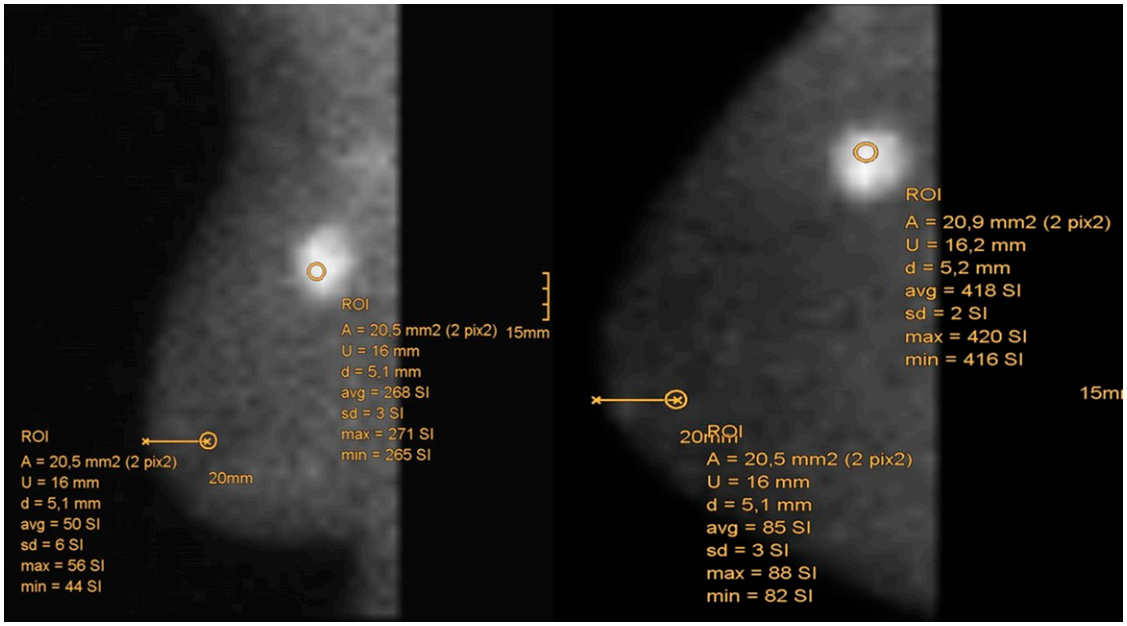

Figure 2. Pie charts illustrating the distribution of histopathology, grading of lesions (G) and breast imaging reporting and data system (BI-RADS®) category. Well differentiated (G1), moderately differentiated (G2), undifferentiated (G3), benign lesions, not assessed in G-categories (NA).

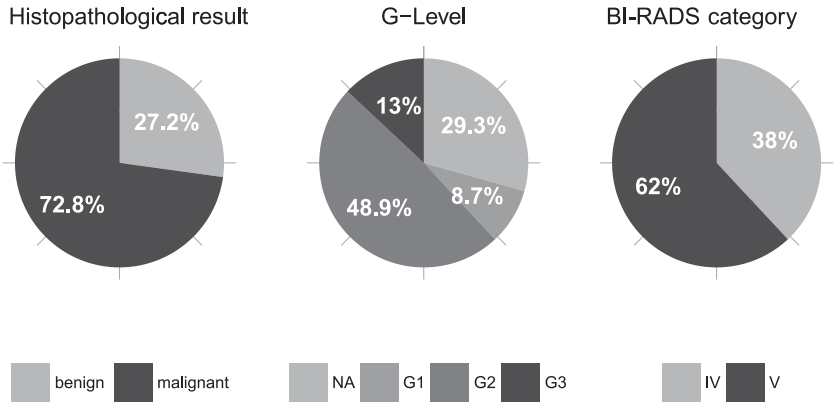

EXAMINATION TECHNIQUES

Clinical examination

At presentation, the clinical history was obtained for all patients, followed by inspection and palpation of both breasts. External breast imaging examinations and written external reports were available at the time of presentation.

Mammography

All mammograms (MG) were performed in accordance with the guidelines and the technical requirements of the national screening program (digital MG using storage plate or full-field digital detector is mandatory).[8] Compliance with the internationally accepted dose limit of 3.0 mGyy delivered by a single craniocaudal (cc) view was ensured.[9] After digital transmission into our imaging archive (IMPAX®; Agfa, Bonn, Germany), mammograms were evaluated on dedicated workstations.

Breast ultrasound

For the ultrasound examination, we used high-end equipment (Voluson E8; GE Healthcare, Chalfont St Giles, UK, or Aixplorer® Expert Edition, SuperSonic, Aix-en Provence, France). Both breasts were examined using a high-frequency (12–18 MHz), high-resolution linear array transducer in radial and antiradial directions. All findings were documented in two perpendicular planes.

Breast-specific gamma imaging

For BSGI, 740–1100 MBq (20–30 mCi) (mean, 843.8 MBq; 22.8 mCi) ^{99m}Tc SestaMIBI (CarioTOP; National Centre for Nuclear Research, Otwock, Poland) were injected in an upper extremity vein contralateral to the affected breast according to the guidelines of the EANM. According to International Commission on Radiological Protection (ICRP) number 80, the estimated absorbed effective radiation dose was 0.0085 mGy MBq^{-1}.[2,10] As there was no suspicion of bilateral breast cancer at the time of BSGI, application via a pedal vein was not performed. There were no hypersensitivity reactions. In all patients, the BSGI was performed before biopsy, since recent diagnostic or therapeutic invasive procedures can cause false-positive SestaMIBI uptake.[2]

Scintigrams of both breasts were performed 10 min after tracer administration with a dedicated gamma camera for BSGI Dilon 6800 (Dilon Technologies, Newport News, VA). In BSGI, the distribution of emitted photons was depicted in cc and mediolateral-oblique

Table 1. Diagnostic performance of imaging modalities ($n = 92$). Results including confidence intervals are listed

Performance	Mammography	Breast ultrasound	MRI	Breast-specific gamma imaging
Sensitivity/TPR[a]	0.85 ± 0.07 (57/67)	0.99 ± 0.02 (66/67)	0.88 ± 0.07 (59/67)	0.90 ± 0.06 (60/67)
Specificity/TNR[a]	0.28 ± 0.09 (7/25)	0.20 ± 0.08 (5/25)	0.40 ± 0.10 (10/25)	0.56 ± 0.10 (14/25)
Precision/PPV[a]	0.76 ± 0.09 (57/75)	0.77 ± 0.09 (66/86)	0.80 ± 0.08 (59/74)	0.85 ± 0.07 (60/71)
NPV[a]	0.41 ± 0.10 (7/17)	0.83 ± 0.08 (5/6)	0.56 ± 0.10 (10/18)	0.67 ± 0.10 (14/21)
Accuracy[a]	0.70 ± 0.09 (64/92)	0.77 ± 0.09 (71/92)	0.75 ± 0.09 (69/92)	0.80 ± 0.08 (74/92)
AUC (*p*-value)	0.64 (0.095)	0.59 (0.041)	0.57 (0.047)	0.73
Kappa	0.15	0.24	0.31	0.48
McNemar	0.19	0.00	0.21	0.48

AUC, area under curve or balanced accuracy with *p*-values from DeLong's test for receiver operating characteristic curves compared with breast-specific gamma imaging; McNemar, *p*-value for comparison of imaging modalities and histologically confirmed results; NPV, negative predictive value (describes the ability of a negative test to rule out malignancy); PPV, positive-predictive value (describes the ability of a positive test to predict malignancy); TNR, true negative rate; TPR, true positive rate.
[a]Numbers for calculation in parenthesis.

Figure 3. Relationship between lesion size and sensitivity of breast-specific gamma imaging (BSGI).

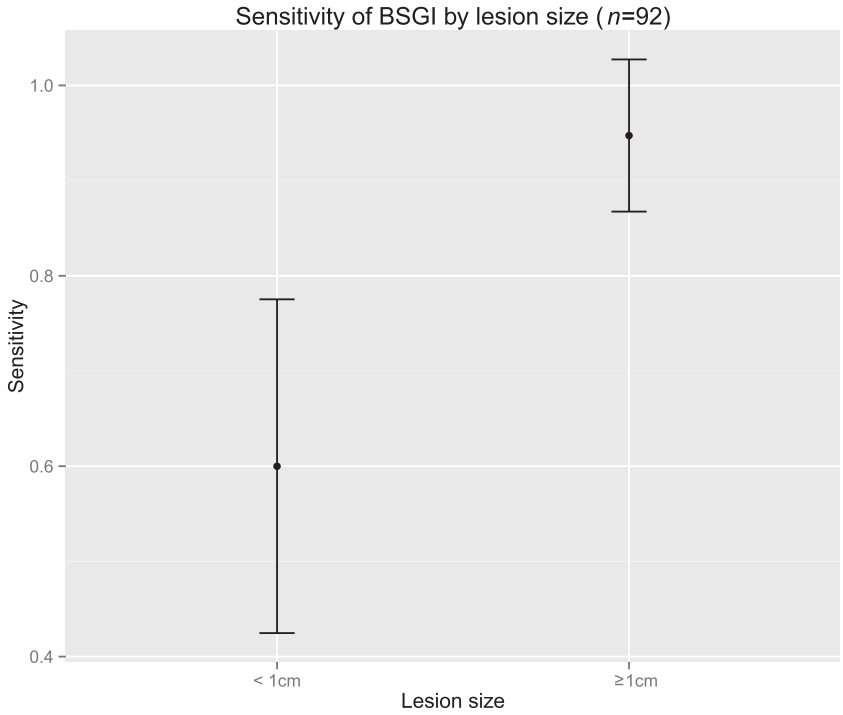

(mlo) projections, comparable to MG. This facilitated comparison with MG. Technical parameters of Dilon gamma camera included 3068 NaI crystals to 3 mm^2 in a 64 × 48 detector matrix connected with position-sensitive photomultiplier tubes (PS-PMT) and resulting in a 152 × 203-mm (6 × 8-inch) area of imaging. The intrinsic resolution of this system was 3.3–4.7 mm, the extrinsic resolution was 6 mm at a distance of 3 cm from the detector.[11] We used a low-energy general-purpose collimator. A 15° slant-hole collimator for imaging breast lesions close to the chest wall, as proposed by Jones et al,[12] was not applied. Special attention was paid on correct patient positioning and avoiding motion artefacts. The total acquisition time did not exceed 40 min, that is to say 6–10 min per projection with a minimum count number of 100.000. Scintigrams were consecutively transmitted to the electronic image archive and assessed visually and semi-quantitatively. Tracer distribution was assessed in a five-category system similar to the BI-RADS according to Brem et al.[13] For semi-quantitative calculation of the relative uptake, a total of four circular regions of interest (ROIs), each 20 mm^2 in size, were placed on the workstation in each projection. One ROI was placed in the area of the highest count number within the clearly definable methoxyisobutylisonitrile accumulation; the ROI of the reference region was always placed 2 cm dorsal to the nipple in an unsuspicious area. This was carried out for cc and mlo projections (Figure 1). The relative uptake factor was calculated according to the ratio:

$$X = \frac{C_{maxL}}{C_{maxBG}}$$

where C_{maxL} is the maximum count number in the lesion and C_{maxBG} is the maximum count number of the ipsilateral parenchymal background.

Any focal radiotracer uptake was correlated with MG and ultrasound, respectively.

Breast MRI

Breast MRI was performed on a 3-T scanner (Achieva®; Philips Healthcare, Best, Netherlands). A dedicated phased-array breast coil with patients in the prone position was used. After

Table 2. Descriptive statistics comparing lesion size and uptake factor (*X*) according to breast imaging reporting and data system (BI-RADS)® categories, rating of the lesions as malignant or benign and grading

Number of lesions	*n* (%)	Lesion size[a]	Uptake factor
		Mean ± CI	Mean ± CI
Total	92	18.27 ± 2.23	3.98 ± 0.52
Malignant	67 (72.8)	18.42 ± 2.30	4.27[b] ± 0.64
Benign	25 (27.2)	17.88 ± 5.51	2.37[b] ± 0.18
BI-RADS IV	35 (38.0)	16.49 ± 4.04	2.43[c] ± 0.15
BI-RADS V	57 (62.0)	19.39 ± 2.60	4.50[c] ± 0.72
G1 level	8 (12.3)	18.00 ± 6.20	3.96 ± 1.25
G2 level	45 (69.2)	17.73 ± 3.04	3.98 ± 0.69
G3 level	12 (18.5)	20.36 ± 3.80	5.63 ± 2.14

CI, confidence interval; levels: G1, well differentiated; G2, moderately differentiated; G3, undifferentiated.
[a]Based on 91 cases, as 1 outlier with a lesion size of 120 mm has been excluded.
[b]Significant mean difference between benign and malignant (Welch two-sample *t*-test, $t = -5.094$, degrees of freedom (df) = 68.956, $p = 0.000$; CI, −2.87 to −1.29).
[c]Significant mean difference between BI-RADS IV and BI-RADS V cases (Welch two-sample *t*-test, $t = -5.254$, df = 59.545, $p = 0.000$; CI, −2.64 to −1.15).

Figure 4. Scatter plot of relative uptake. In our series, 3.04 could be considered as a threshold for relative uptake (*X*), which was only exceeded by malignant lesions. If a lesion is detectable in breast-specific gamma imaging (BSGI), lesion size is irrelevant for *X*.

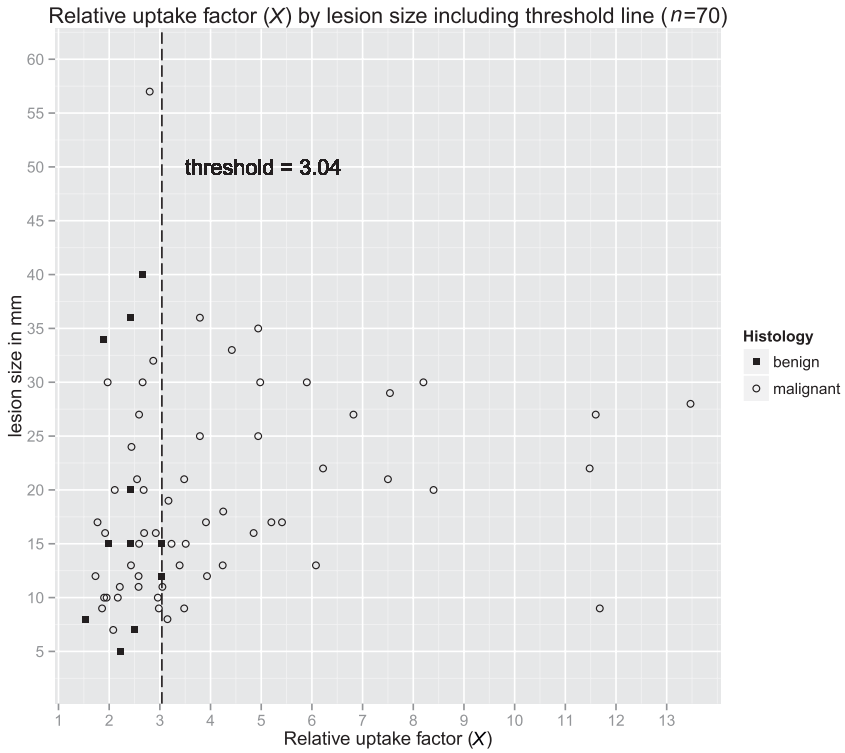

T_2 weighted fat-suppressed images [echo time (TE)/repetition time (TR)/inversion recovery (IR), 60/9065/230 ms; slice thickness, 3 mm; field of view (FOV), 32–40 cm; total measuring time, 3.37 min], diffusion-weighted images (TE inversion recovery (TR), 59/8157 ms; *b*-values, 0/600 ms; slice thickness, 3 mm; total measuring time, 3.07 min) were obtained. Finally, four T_1 weighted

Figure 5. Error bar chart of mean relative uptake in ductal cancers and other malignant entities. IDC, invasive ductal carcinoma; DCIS, ductal carcinoma *in situ*.

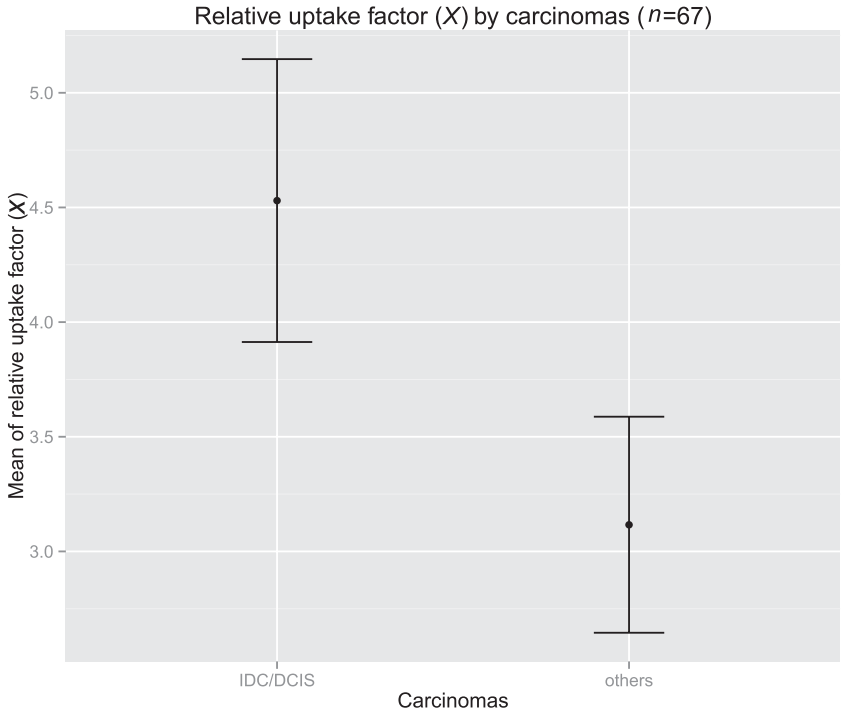

fat-suppressed dynamic acquisitions (TE/TR, 2.3/4.1 ms; slice thickness, 1 mm; measuring time per volume/total measuring time, 56.6 ms/7.33 min) were performed for the period of 5 min after intravenous administration of the contrast media. All sequences were acquired in the axial scan direction. As contrast agent, we used either 15-ml gadoteric acid (DOTAREM®; Guerbet, Cedex, France) or 7-ml gadobutrol (GADOVIST®; Bayer Schering Pharma, Berlin, Germany). Flow rates were 2.5 and 1.0 ml s^{-1}, respectively, followed by a saline bolus (30 ml). Kinetic analysis was performed on a workstation placing circular ROIs around a lesion to calculate time–intensity curves.

Biopsy techniques

All 92 lesions underwent image-guided biopsy. For biopsy planning, the results of all imaging modalities were available. 90 of the 92 lesions could be biopsied with sonographic guidance. A 14-gauge automated biopsy system (Magnum®; Bard®, Tempe, AZ) was used in coaxial technique *via* a 13-gauge biopsy needle (TrueGuide®; Bard®). Two lesions in different patients with microcalcifications could not be visualized with ultrasound, and therefore, stereotactic vacuum-assisted biopsy had to be performed in prone positioning on a digital stereotactic table (Lorad Multicare Platinum; Hologic, Danbury, CT) using a 9-gauge probe (Suros Eviva®; Hologic). Radiographs were performed of the specimen in order to prove calcifications. In all 92 lesions, a site marker (HydroMARK®; Biopsy Sciences, Clearwater, FL) was placed in the lesion, and its position was verified in MG.

There were no biopsy-related complications. Histopathological results were correlated with imaging findings for concordance.

STATISTICAL ANALYSIS

The BI-RADS categories for each modality and the final BI-RADS category as well as the calculated relative uptake values were noted in an Excel® spreadsheet (Microsoft Corporation, Redmond, WA). Based on the results of the reference standard, sensitivity, specificity, positive-predictive and negative-predictive values, and accuracy were calculated for BSGI and for the morphological imaging modalities.

Furthermore, the area under the curve (AUC) was calculated, because it is particularly suitable to summarize the reliability of imaging modalities in one parameter as the mean of sensitivity and specificity. Consequently, the different imaging modalities can be statistically compared with reference to a single estimate. Variations in AUC values have been assessed with a DeLong's difference test providing significant differences between the AUC values. To validate the results of AUCs, Cohen's kappa was calculated, which describes the accordance of imaging and

Figure 6. (a–e) Characterization of mass lesions with breast-specific gamma imaging (BSGI). Thick arrows in (a–c) and (e) point to invasive ductal carcinoma behind the left nipple, thin arrows in (a, b and d) point to circumscribed breast parenchyma with fibrosis. Dashed ellipses in (e) encircle the region of upper outer quadrant without tracer uptake (assumed position of second lesion). (a, b) Mammograpy craniocaudal (cc) (a) and mediolateral oblique (mlo) (b) projections; (c) three-dimensional (3D) ultrasound of carcinoma behind the nipple; (d) 3D ultrasound of breast parenchyma with fibrosis; (e) planar BSGI in cc (figure above) and mlo (figure below) projections.

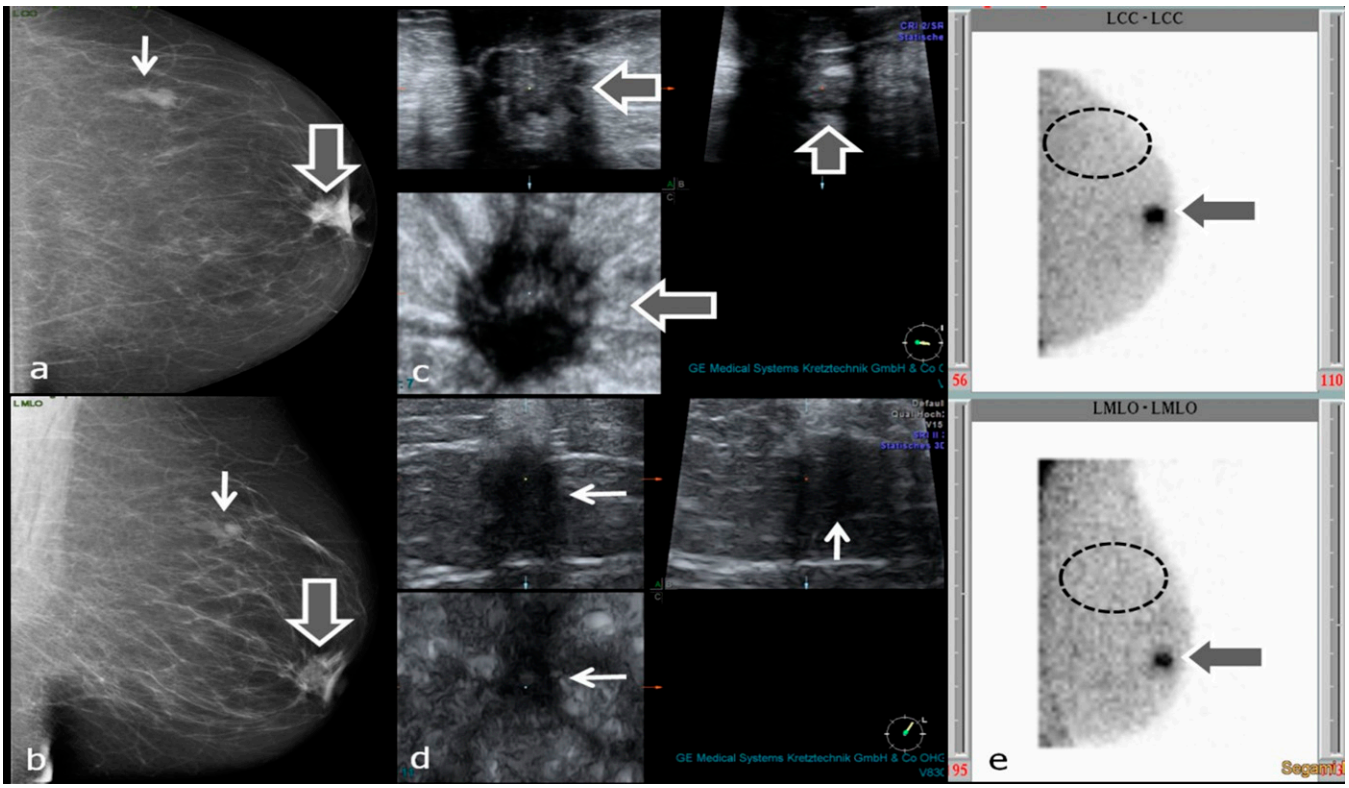

histopathological findings in a range between zero (accidental agreement) and one (perfect match). In addition, McNemar test was performed for paired samples to determine the significance of disagreement between imaging and histopathological findings. In contrast to sensitivity and specificity, which describe the specific performance of an imaging modality, Cohen's kappa and McNemar provide a statistical comparison between the imaging studies and the histopathological examinations. AUC, Cohen's kappa and McNemar test together are the profound basis for overall assessment of imaging and histopathological findings, exceeding separate analysis of sensitivity and specificity. Analysis and graphics were created with R 3.0.3,[14] as well with the packages psych,[15] pROC[16] and ggplot2.[17] Wilcoxon test was used to illustrate different relative uptake (X) of highly *vs* moderately and poorly differentiated carcinomas. Welch two-sample t-test was used to calculate the differences between the relative uptake factors of malignant *vs* benign lesions as well as between the different types of cancers.

RESULTS

In 67 patients with a mean age of 64 years, 92 suspicious lesions (BI-RADS IV and V) were diagnosed with MG and ultrasound and included in this lesion-based analysis. In 47 (70%) patients, 1 suspicious lesion was detected; in 15 (22%) patients, 2 suspicious lesions were detected; and in 5 (7%) patients, 3 lesions were detected. Eight patients (9%) had synchronous bilateral suspicious findings. Among the 92 lesions, 35 (38%) were assessed as BI-RADS IV and 57 (62%) were assessed as BI-RADS V. Histopathological examination of these pre-selected lesions revealed 67 (72.8%) malignant and 25 (27.2%) benign lesions. Among the 67 malignancies, 64 (95.5%) were invasive cancers and 3 (4.5%) were carcinomas *in situ*. 53 of the invasive cancers were invasive ductal type (= no specific type), and 11 lesions were other entities (lobular, tubulo-lobular carcinomas). Lesion diameters were measured in the morphological imaging modality (MG, ultrasound or MRI) in which the lesion was best visualized. Average diameter of histologically proven benign lesions was 17.88 mm and that of malignant lesions was 18.42 mm. In 65 of the 67 cancers, grading was assessed in histopathological examination [in 1 case with Paget's disease and 1 ductal carcinoma *in situ* (DCIS) grading was not determined]. 8 of these 65 malignant lesions were well differentiated (G1), 45 were moderately differentiated (G2) and 12 were undifferentiated (G3). Among the BI-RADS IV lesions, 11 (31.4%) were histopathologically assessed as malignant, among the

Figure 7. (a–c) Characterization of breast calcifications with breast-specific gamma imaging (BSGI). Dotted triangles in mammograms (MGs) (a, b) surround microcalcifications. In (c), dotted triangles surround the assumed location of calcifications in BSGI. (a, b) Magnifications of MGs craniocaudal (cc) (a) and mediolateral oblique (mlo) (b); (c) BSGI in cc (figure above) and mlo (figure below) projection. RCC, right craniocaudal; RMLO, right mediolateral oblique.

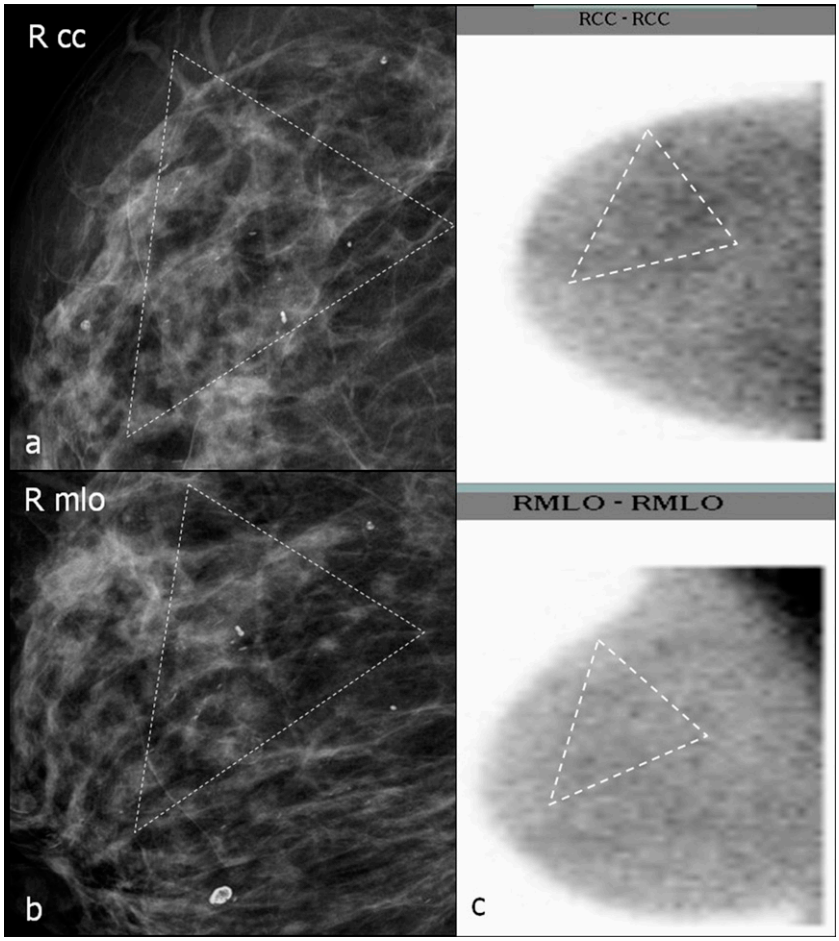

BI-RADS V lesions 56 (98.2%) were malignant (Figure 2). The latter results are consistent with the recommendations of BI-RADS providing a likelihood of cancer between 2% and 95% for lesions of the Category IV and >95% for lesions of the Category V.[7]

The sensitivity of ultrasound to detect malignant lesions reached 99% (66 of the 67 cancers) and thus was superior to BSGI (90%, 60 of the 67 cancers), MRI (88%, 59 of 67 cancers) and MG (85%, 57 of 67 cancers). However, specificity of ultrasound was the lowest (20%, 5 of the 25 benign lesions) compared with MG (28%, 7 of the 25 benign lesions), MRI (40%, 10 of the 25 benign lesions) and BSGI (56%, 14 of the 25 benign lesions). Correspondingly, positive-predictive value for malignancy of a lesion, accuracy and AUC were the highest for BSGI (85%, 80% and 0.73%, respectively). The AUC for each imaging modality highlights the outstanding diagnostic potential of BSGI (0.73) compared with MG (0.64), ultrasound (0.59) and MRI (0.57) in our diagnostic approach. Compared with BSGI (80%), the accuracy of MRI (75%) was not significantly lower in contrast to its AUC (0.73 *vs* 0.57). Hence, Cohen's kappa for BSGI (0.48) was higher than those of other modalities (MRI, 0.31; ultrasound, 0.24; MG, 0.15) (Table 1). McNemar's test suggests a highly significant difference between the results of ultrasound and the histopathological examination, despite its highest sensitivity.

The sensitivity of BSGI for the 19 lesions with a diameter of <1 cm was significantly lower with an average of 60%. Among the lesions <1 cm, 11 (57.9%) were malignant, 3 were well differentiated (G1) and 8 were moderately differentiated (G2). In contrast to all G1 carcinomas, two G2 carcinomas <1 cm could not be detected with BSGI. Among the benign lesions <1 cm, six (31.5%) were not demarcated in BSGI. Considerable uncertainty in the estimated sensitivity is reflected by the large confidence interval (CI).

However, lesions exceeding 1 cm were detected with an average sensitivity of 94% (Figure 3). Assuming a threshold of 1 cm for

Figure 8. (a–e) Occult breast carcinoma in breast-specific gamma imaging (BSGI) and mammography (MG) owing to eccentric location. Thick arrows in (c, d) point to breast carcinoma at the right parasternal chest wall that was only found with ultrasound and MRI owing to its eccentric location. Star in (d) marks malignant haemorrhagic pleural effusion. Dashed rectangles in (a, b and e) highlight the inner lower quadrant of right breast with no lesion detectable. (a, b) MGs craniocaudal (cc) (a) and mediolateral oblique (mlo) (b); (c) ultrasound of the right-sided cancer; (d) MRI T_1 weighted FS + DOTAREM® (Guerbet, Cedex, France); (e) BSGIs in cc (figure above) and mlo (figure below) projection. RCC, right craniocaudal; RMLO, right mediolateral oblique.

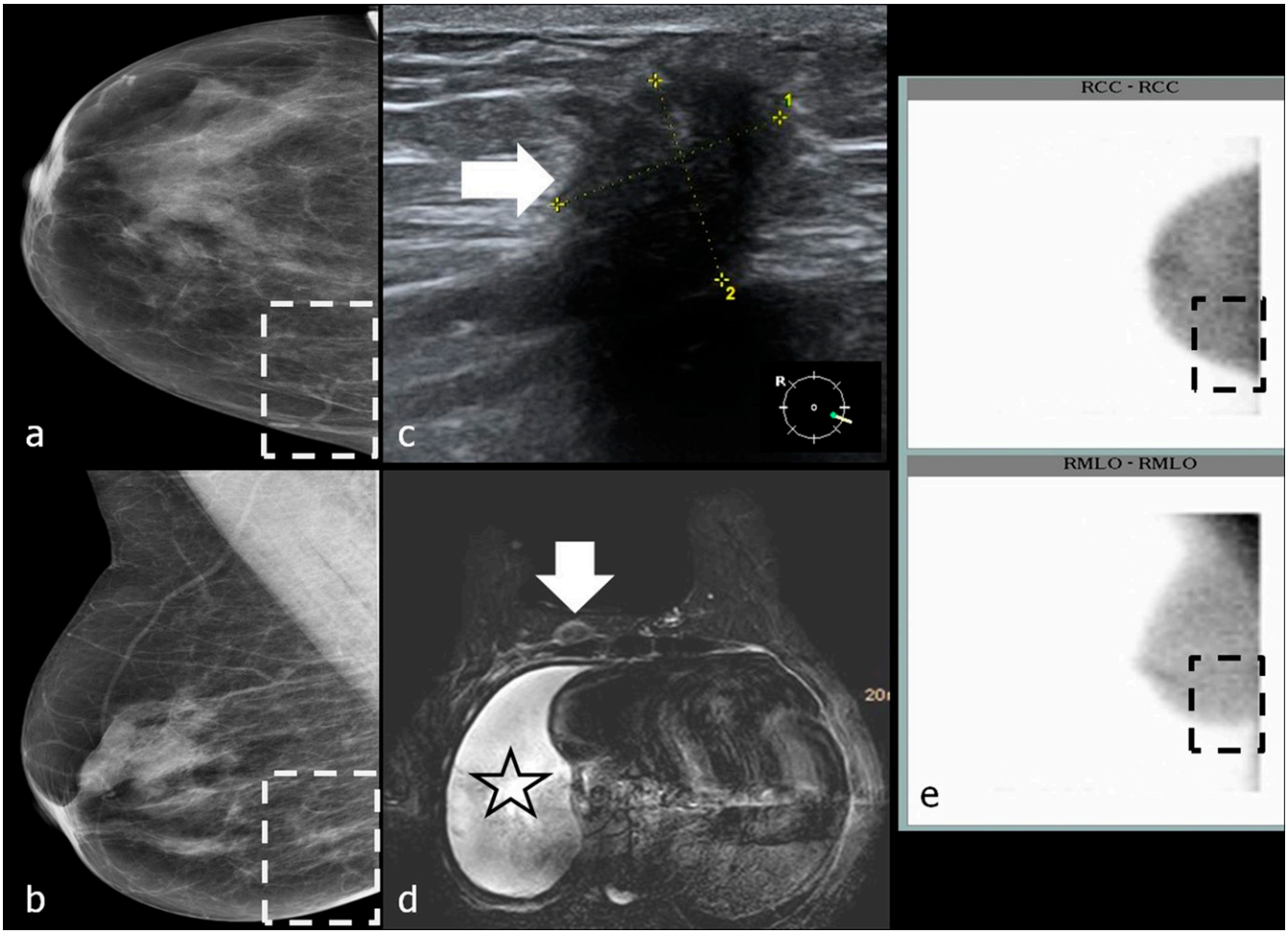

detecting a breast lesion with BSGI reliably, BSGI could be used for characterization of lesions detected in MG and ultrasound. Six of eight lesions were correctly negative in BSGI (Scores 1 and 2). Only one case of a DCIS and another case of an invasive ductal carcinoma (IDC), both exceeding 1 cm, were false negative in BSGI. The IDC was not detectable in BSGI and MG because of its eccentric location (see also limitations).

The relative uptake (X) was significantly higher for malignant lesions (mean, 4.27) than for benign lesions (mean, 2.37; $p < 0.001$) (Table 2). $X > 3.04$ was only calculated in malignant lesions, independently from its size (Figure 4).

Among malignant lesions, average relative uptake differed significantly between ductal types (mean, 4.53; DCIS and IDC) and the other histopathological entities (mean, 3.12, lobular, tubular and tubulolobular carcinomas; Figure 5).

Concerning the grading of carcinomas, X differed not significantly between high-grade (G3) and lower grade (G1 and G2) carcinomas ($p = 0.02408$; Wilcoxon test), independently of the lesion diameter (Table 2).

DISCUSSION

In our study, the BSGI was used and interpreted as an adjunct to MG and ultrasound in the work-up of suspicious breast lesions in a breast cancer centre. Additionally, for all lesions, MRI and finally biopsy as the reference standard were performed. Patients, both asymptomatic and with pain or palpation findings were either imaged at our institution or referred to our university hospital breast imaging section for further evaluation following external examinations. In an assessment centre for breast lesions, the ideal imaging modality should be characterized by a high sensitivity, high specificity and, particularly, a high positive-predictive value for malignancy. Although imaging findings cannot replace biopsy, additional characterization of breast lesions with BSGI may contribute to a more focused work-up. The decision to biopsy a breast lesion and the selection of the lesion subjected to biopsy—in cases of more than one lesion—can be facilitated. Complications of biopsy, such as haematomas or infections could be avoided; however, more widespread use may be impeded by the fact that patients need to be injected with a radiopharmaceutical substance.

In our study, the BSGI appears to be valuable for the characterization of lesions detected in MG and ultrasound (Figure 6) owing to a high positive-predictive value and specificity for the diagnosis of malignant lesions compared with the morphological imaging modalities. However, morphological imaging modalities are superior to BSGI in the detection of smaller lesions owing to a higher spatial resolution (Table 1, Figure 3). Therefore, BSGI does not contribute to local staging. In contrast to older scintimammography studies, we performed BSGI with a dedicated small FOV gamma camera.[18] The development of

Figure 9. (a–e) Breast-specific gamma imaging (BSGI)-occult, small left-sided carcinoma (G2). Left breast was assessed as Category 2 according to Brem et al.[13] Larger right-sided carcinoma (18 mm) was clearly seen as focal spot on scintigram. Thick arrows in (a, b, d and e) point to 4-mm left-sided carcinoma. Thin arrows in (a–c) mark the 18-mm right-sided carcinoma. (a, b) Bilateral mammograms craniocaudal (cc) (above) and mediolateral oblique (mlo) (below); (c) BSGIs of both breasts in cc (figure above) and mlo (figure below) projections; (d) MRI of the left breast, T_1 weighted FS + DOTAREM® (Guerbet, Cedex, France); (e) ultrasound of the left-sided cancer. LCC, left craniocaudal; LMLO, left mediolateral oblique; RCC, right craniocaudal; RMLO, right mediolateral oblique.

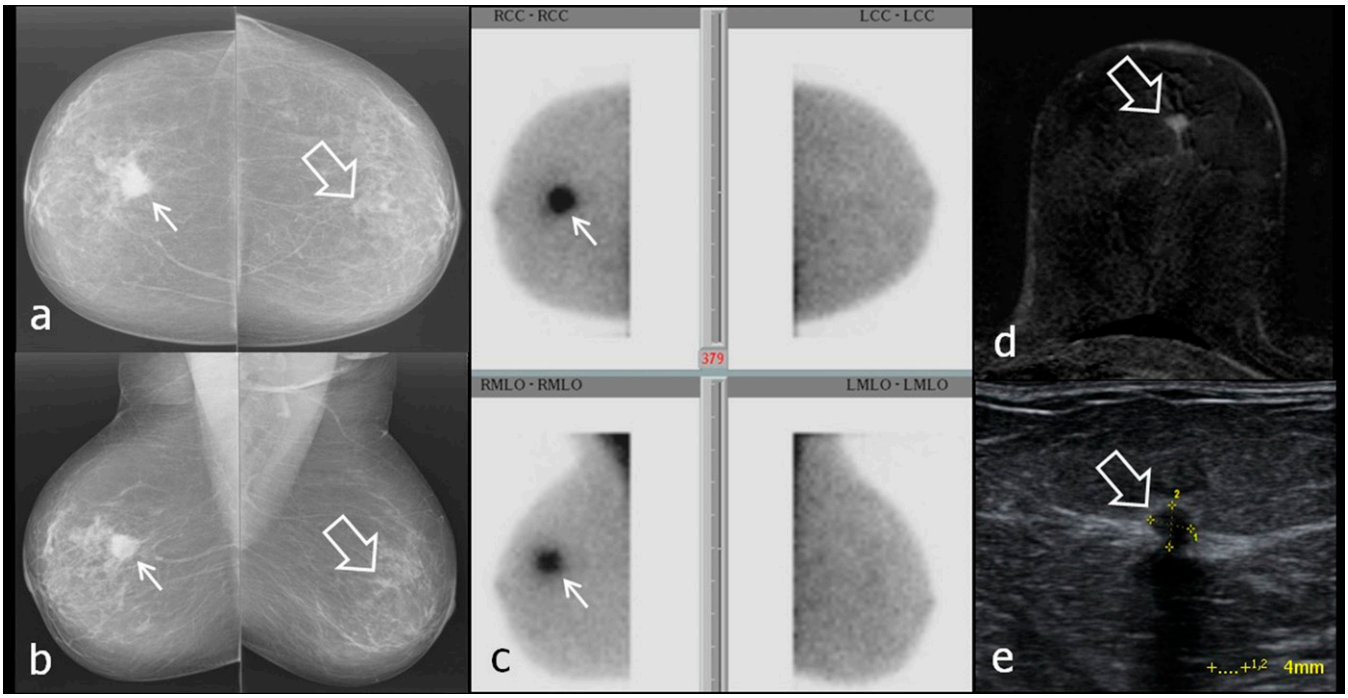

these cameras increased the spatial resolution and enabled an exact spatial correlation of BSGI findings with MG.

Characterization of breast lesions with breast-specific gamma imaging

Our data show the high sensitivity of MG and ultrasound for lesion detection (85% and 99%, respectively). However, since only 28% (MG) and 20% (ultrasound) of histopathologically proven benign lesions were correctly diagnosed as unsuspicious and positive-predictive values for malignancy for both modalities were comparatively low (76% MG; 77% ultrasound), characterization of lesions only with these modalities may be inconclusive.

A sensitivity of 88% and positive-predictive value for malignancy of 80% for breast MRI in our patient population is consistent with the current literature.[19] However, MRI analysis was more time consuming than the analysis of the four scintigrams.

Sensitivity of BSGI was acceptable (90%) and only slightly lower than the study of Brem et al,[13] who also employed a NaI detector coupled to a PS-PMT. In our study, specificity of BSGI was higher than the other modalities but significantly lower than in the study of Kim.[20] However, we evaluated the role of BSGI as an adjunct to MG and ultrasound in suspicious lesions, and BSGI interpretation was not blinded to the findings of MG and ultrasound.

The BSGI can not only help in the characterization of a breast lesion but also in the selection of a target for biopsy in the case of more than one lesion because of its high positive-predictive value for malignancy, and *vice versa* its high negative-predictive value of an unremarkable study.

As early as in 2002, Lumachi et al[21] prospectively evaluated a positive-predictive value (PPV) of 95.1% for non-palpable, mammographically detected suspicious breast lesions using large FOV scintimammography. In our opinion, the lower PPV (85%) of BSGI in our study could be the result of the larger number of small lesions in our study or a higher rate of malignant lesions with only moderately elevated tissue metabolism (relative uptake factor <3.04).

In one patient, two lesions in the left breast, one behind the nipple and the other in the upper outer quadrant, were found, and both were suspicious in MG and ultrasound. Increased ^{99m}Tc SestaMIBI uptake was only observed in the lesion behind the nipple, which proved to be an IDC (Figure 6). The second lesion was unsuspicious breast parenchyma with fibrosis. In one patient, ductal microcalcifications in the right breast without ^{99m}Tc SestaMIBI uptake proved to be granulomatous galactophoritis (Figure 7).

Breast-specific gamma imaging relative uptake factor (*X*)

By calculating a relative uptake factor (*X*), specificity and accuracy of BSGI could be increased if a lesion could be detected unequivocally and a ROI be placed precisely. In our study, all breast lesions with *X* exceeding 3.04 proved to be malignant and should be categorized as BI-RADS 5 (Figure 4).

Figure 10. (a, b) Small, breast-specific gamma imaging (BSGI)-negative ductal carcinoma *in situ* in the right upper outer quadrant. Dashed ellipses encircle microcalcifications. Ellipses in (b) mark the expected location of microcalcifications in BSGI. No Technetium-99m SestaMIBI uptake could be seen. (a) Mammogram [craniocaudal (cc)], magnification view; (b) BSGI in cc (figure above) and mediolateral-oblique (figure below) projection. LCC, left craniocaudal; LMLO, left mediolateral oblique.

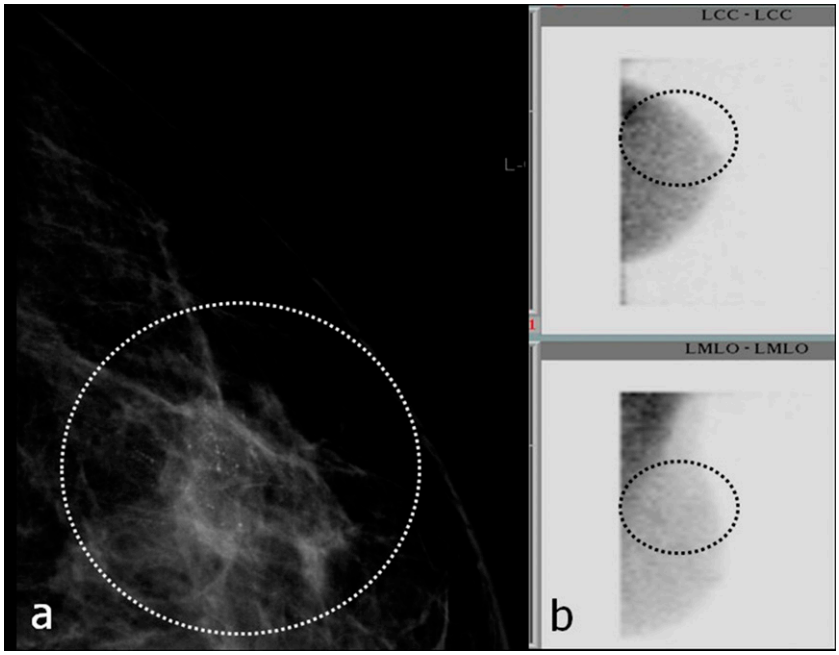

^{99m}Tc SestaMIBI is a lipophilic cationic compound and a member of the chemical isonitrile family. Being lipid soluble, it diffuses unspecifically from the blood into the cytoplasm and the mitochondria and is retained in the region of the mitochondria because of its negative transmembrane potential.[22] Uptake and retention of ^{99m}Tc SestaMIBI depend on angiogenesis and regional perfusion, plasma and mitochondrial membrane potentials and thus the level of tissue metabolism.[23] Increased relative uptake factor of high-grade breast cancers can be explained by upregulated angiogenesis, increased perfusion and hyperproliferation.[24,25] Similarly to the results of fluorine-18 fludeoxyglucose positron emission tomography examinations of the breast, relative uptake of ^{99m}Tc SestaMIBI in the 11 cases with lobular and tubulolobular carcinomas was lower than in the ductal types.[26]

In contrast to the study of Park et al,[27] we have calculated the relative uptake factor of a lesion relative to the background activity in the ipsilateral breast. In our opinion, influencing factors such as differences in positioning of the breasts on the detector or a varying background activity owing to asymmetry of glandular tissue are less significant using our method.

By using the absolute count numbers in an exactly defined ROI, significant fluctuations of standard deviations in count numbers within small ROIs can be neglected. In contrast to Hruskaa and O'Connor[28] who used a dedicated breast imaging system comprising two identical opposing cadmium zinc telluride detectors, our calculation method only results in an approximate relative uptake factor, because the size of a lesion, its distance from the detector and the breast thickness are not taken into account.

Figure 11. (a–e) A breast-specific gamma imaging (BSGI) negative, breast imaging reporting and data system (BI-RADS®) IVa lesion (indistinct lateral margins in ultrasound) in the left breast. Histopathological examination confirmed fibroadenomatosis. Thick arrows in (a–d) point to the BI-RADS IVa lesion, thin arrows in (c) mark the indistinct margins of the lesion in ultrasound. Dashed ellipses in (e) mark the expected location of the lesion in scintigram. (a, b) Mammography (MGs) of the left breast craniocaudal (cc) (above) and mediolateral-oblique (mlo) (below) projection; (c) ultrasound of the BI-RADS® IVa lesion; (d) MRI of the left breast, T1wFS + DOTAREM® (Guerbet, Cedex, France); BSGIs of the left breast in cc (figure above) and mlo (figure below) projection. LCC, left craniocaudal; LMLO, left mediolateral oblique.

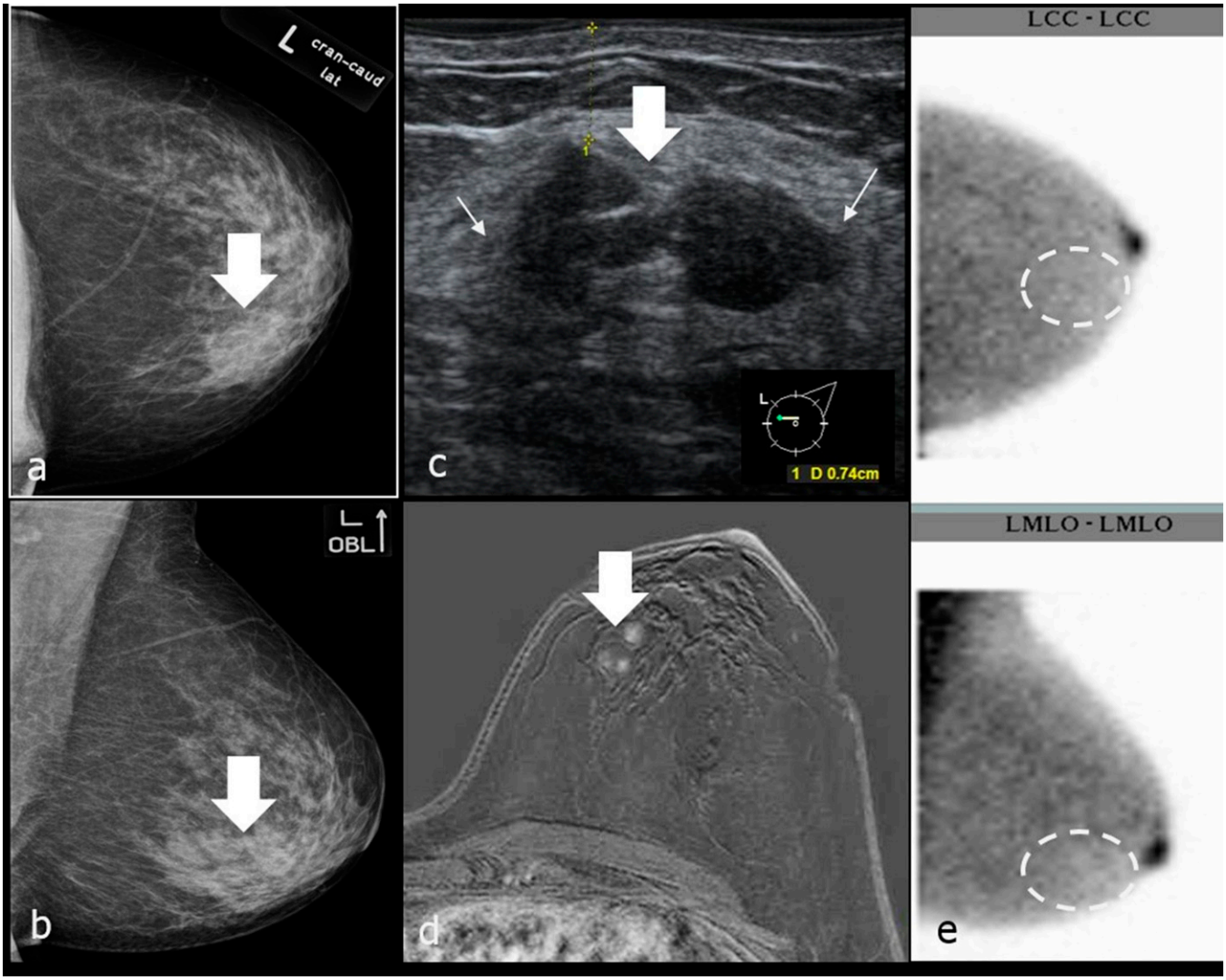

However, we believe that our method is easier to use in daily practice and increases the diagnostic validity of BSGI.

Limitations of breast-specific gamma imaging

For correct interpretation of BSGI, findings of previous MG and ultrasound have to be taken into account. In two patients, carcinomas could not be detected with BSGI because of their eccentric parasternal location and thus could not be positioned within the FOV of the BSGI camera. But these lesions were not depicted on MG either.

Similar limitations were described by Spanu et al.[29] In a 60-year-old patient, a histopathologically proven carcinoma in right parasternal location was occult in BSGI and MG (Figure 8).

There is a drop in sensitivity of BSGI for lesions with a diameter of <1 cm (60%; CI, 42.7–77.5%), so BSGI is limited in the detection of small cancers (Figure 9). In another study using the same type of camera reported sensitivity for smaller lesions was higher.[30] We could demonstrate that non-visualization of malignant lesions in BSGI is either owing to small size (<1 cm) or owing to better tumour grade (G1 *vs* G2 or 3). However, in our study most of the malignant lesions measuring <1 cm (8/11) were moderately differentiated (G2).

The high specificity of BSGI for characterization of microcalcifications of 90% (in 9 of 10 cases unsuspicious microcalcifications were correctly assessed) correlated with the data of Brem et al.[30] In one patient, a small DCIS was not recognized in BSGI (Figure 10). Also, Park et al[27] point out the decreased sensitivity of BSGI for small DCIS. These cases demonstrate limitations of sensitivity not only of BSGI, but also of morphological imaging modalities. Small lesions for example, as shown in Figure 9, may not be detectable in MG. Microcalcifications are usually missed in ultrasound.

Therefore, BSGI should only be considered as unsuspicious, if concordance with findings of other modalities has been obtained. Only in these cases, image-guided biopsy can be waived, as also postulated by Zhou et al.[31]

In our opinion and according to the data of this study, BSGI negativity may support the decision not to biopsy in lesions with low or moderate prevalence for malignancy (BI-RADS III or IVa lesions), that is to say a likelihood for cancer of up to 10% (Figure 11).[7] In addition, a negative BSGI (Scores 1 and 2) may also obviate the need for biopsy in lesions >1 cm without microcalcifications.[32]

CONCLUSION

In an assessment centre, BSGI can be a valuable tool for the work-up of suspicious breast lesions detected in MG and ultrasound. It can help in the characterization and classification of breast lesions according to BI-RADS. The measurement of a relative uptake factor (X), which can be calculated easily, increases the diagnostic potential of BSGI. BSGI should always be assessed in synopsis with the other imaging modalities, as was carried out in our study. As an adjunct to MG and ultrasound, BSGI negativity may obviate the need for biopsy of lesions with a low or moderate prevalence for malignancy (BI-RADS III and BI-RADS IVa) and in lesions >1 cm and without microcalcifications.

REFERENCES

1. Berg WA, Gutierrez L, NessAiver MS, Carter WB, Bhargavan M, Lewis RS, et al. Diagnostic accuracy of mammography, clinical examination, US, and MR imaging in preoperative assessment of breast cancer. *Radiology* 2004; **233**: 830–49. doi: 10.1148/radiol.2333031484
2. Bombardieri E, Aktolun C, Baum RP, Bishof-Delaloye A, Buscombe J, Chatal JF, et al. Breast scintigraphy: procedure guidelines for tumour imaging. *Eur J Nucl Med Mol Imaging* 2003; **30**: 107–14.
3. Khalkhali I, Mena I, Diggles L. Review of imaging techniques for the diagnosis of breast cancer: a new role of prone scinti-mammography using technetium-99m sestamibi. *Eur J Nucl Med* 1994; **21**: 357–62. doi: 10.1007/BF00947973
4. Liberman M, Sampalis D, Mulder DS, Sampalis JS. Breast cancer diagnosis by scinti-mammography: a meta-analysis and review of the literature. *Breast Cancer Res Treat* 2003; **80**: 115–26. doi: 10.1023/A:1024417331304
5. Hruska CB, O'Connor MK. Nuclear imaging of the breast: translating achievements in instrumentation into clinical use. *Med Phys* 2013; **40**: 050901. doi: 10.1118/1.4802733
6. Tadwalkar RV, Rapelyea JA, Torrente J, Rechtman LR, Teal CB, McSwain AP, et al. Breast-specific gamma imaging as an adjunct modality for the diagnosis of invasive breast cancer with correlation to tumour size and grade. *Br J Radiol* 2012; **85**: 212–16. doi: 10.1259/bjr/34392802
7. D'Orsi CJ, Sickles EA, Mendelson EB, Morris EA. ACR BI-RADS® Altas, Breast Imaging Reporting and Data System. Reston, VA. American College of Radiology; 2013.
8. BKFP-programmbeschreibung. Available from: http://www.bura.at/bkfp-programmbeschreibung/
9. ACR practice guideline for the performance of screening and diagnostic mammography (Resolution 39). Available from: http://www.acr.org/~/media/ACR/Documents/PGTS/guidelines/Screening_Mammography.pdf
10. ICRP. Radiation dose to patients from radiopharmaceuticals (addendum 2 to ICRP publication 53). *Ann ICRP* 1998; **28**: 1–126.
11. *Dilon 6800: technical specifications*. Newport News, VA: Dilon Technologies Inc., 2012.
12. Jones EA, Phan TD, Blanchard DA, Miley A. Breast-specific gamma-imaging: molecular imaging of the breast using 99mTc-sestamibi and a small-field-of–view gamma-camera. *J Nucl Med Technol* 2009; **37**: 201–5. doi: 10.2967/jnmt.109.063537
13. Brem RF, Floerke AC, Rapelyea JA, Teal C, Kelly T, Mathur V. Breast-specific gamma imaging as an adjunct imaging modality for the diagnosis of breast cancer. *Radiology* 2008; **247**: 651–7. doi: 10.1148/radiol.2473061678
14. R-project.org. A language and environment for statistical computing. R Foundation for Statistical Computing [latest R version 3.2.0, released 16 April 2015]. Vienna, Austria:

R Core Team. Available from: http://www.R-project.org
15. R-project.org; Revelle W. Psych: procedures for personality and psychological research Northwestern University. [latest version 1.5.2, released 19 February 2015]. Available from: http://CRAN.R-project.org/package=psych
16. Robin X, Turck N, Hainard A, Tiberti N, Lisacek F, Sanchez JC, et al. pROC: an open-source package for R and S+ to analyze and compare ROC curves. *BMC Bioinformatics* 2011; **12**: 77. doi:10.1186/1471-2105-12-77
17. Wickham H, ed. *ggplot2: elegant graphics for data analysis*. New York, NY: Springer; 2009.
18. Sampalis FS, Denis R, Picard D, Fleiszer D, Martin G, Nassif E, et al. International prospective evaluation of scintimammography with (99m) technetium sestamibi. *Am J Surg* 2003; **185**: 544–9. doi: 10.1016/S0002-9610(03)00077-1
19. Bluemke DA, Gatsonis CA, Chen MH, DeAngelis GA, DeBruhl N, Harms S, et al. Magnetic resonance imaging of the breast prior to biopsy. *JAMA* 2004; **292**: 2735–42. doi: 10.1001/jama.292.22.2735
20. Kim B. Usefulness of breast-specific gamma imaging as an adjunct modality in breast cancer patients with dense breast: a comparative study with MRI. *Ann Nucl Med* 2012; **26**: 131–7. doi: 10.1007/s12149-011-0544-5
21. Lumachi F, Zuccetta P, Marzola MC, Ferretti G, Povolato M, Paris MK, et al. Positive predictive value of 99mTc sestamibi scintimammography in patients with non-palpable, mammographically detected, suspicious, breast lesions. *Nucl Med Commun* 2002; **23**: 1073–8. doi: 10.1097/01.mnm.0000040968.72730.49
22. Chiu ML, Kronauge JF, Piwinca-Worms D. Effect of mitochondrial and plasma membrane potentials on accumulation of hexakis (2-methoxyisobutylisonitrile) technetium(I) in cultured mouse fibroblasts. *J Nucl Med* 1990; **31**: 1646–53.
23. Buscombe JR, Cwikla JB, Thakrar DS, Hilson AJ. Uptake of Tc-99m MIBI related to tumour size and type. *Anticancer Res* 1997; **17**: 1693–4.
24. Mankoff DA, Dunnwald LK, Gralow JR, Ellis GK, Schubert EK, Charlop AW, et al. [Tc-99m]-sestamibi uptake and washout in locally advanced breast cancer are correlated with tumor blood flow. *Nucl Med Biol* 2002; **29**: 719–27. doi: 10.1016/s0969-8051(02)00333-5
25. Scopinaro F, Schillaci O, Scarpini M, Mingazzini PL, Di Macio L, Bianci M, et al. Technetium-99m sestamibi: an indicator of breast cancer invasiveness. *Eur J Nuc Med* 1994; **21**: 984–7. doi: 10.1007/bf00238124
26. Heudel P, Cimarelli S, Montella A, Bouteille C, Mognetti T. Value of PET-FDG in primary breast cancer based on histopathological and immunohistochemical prognostic factors. *Int J Clin Oncol* 2010; **15**: 588–93. doi: 10.1007/s10147-010-0120-3
27. Park KS, Chung HW, Yoo YB, Yang JH, Choi N, So Y. Complementary role of semiquantitative analysis of breast-specific gamma imaging in the diagnosis of breast cancer. *AJR Am J Roentgenol* 2014; **202**: 690–5. doi: 10.2214/AJR.13.11324
28. Hruskaa CB, O'Connor MK. Quantification of lesion size, depth, and uptake using a dual-head molecular breast imaging system. *Med Phys* 2008; **35**: 1365–76. doi: 10.1118/1.2885371
29. Spanu A, Chessa F, Sanna D, Cottu P, Manca A, Nuvoli S, et al. Scintimammography with a high resolution dedicated breast camera in comparison with SPECT/CT in primary breast cancer detection. *Q J Nucl Med Mol Imaging* 2009; **53**: 271–80.
30. Brem RF, Shahan C, Rapleyea JA, Donnelly CA, Rechtman LR, Kidwell AB, et al. Detection of occult foci of breast cancer using breast-specific gamma imaging in women with one mammographic or clinically suspicious breast lesion. *Acad Radiol* 2010; **17**: 735–43. doi: 10.1016/j.acra.2010.01.017
31. Zhou M, Johnson N, Blanchard D, Bryn S, Nelson J. Real-world application of breast-specific gamma imaging, initial experience at a community breast center and its potential impact on clinical care. *Am J Surg* 2008; **195**: 631–5. doi: 10.1016/j.amjsurg.2008.01.006
32. Brem RF, Rapelyea JA, Zisman G, Mohtashemi K, Raub J, Teal CB, et al. Occult breast cancer: scintimammography with high-resolution breast-specific gamma camera in women at high risk for breast cancer. *Radiology* 2005; **237**: 274–80. doi: 10.1148/radiol.2371040758